Titania–Silica Nanocomposite Photocatalysts with Application in Stone Self-Cleaning

ARTICLE *in* THE JOURNAL OF PHYSICAL CHEMISTRY C · NOVEMBER 2011

Impact Factor: 4.77 · DOI: 10.1021/jp2074623

2 AUTHORS, INCLUDING:

María J. Mosquera
Universidad de Cádiz
34 PUBLICATIONS **595** CITATIONS

THE JOURNAL OF PHYSICAL CHEMISTRY C

ARTICLE

pubs.acs.org/JPCC

Titania-Silica Nanocomposite Photocatalysts with Application in Stone Self-Cleaning

Luís Pinho and Maria J. Mosquera*

Departamento de Química-Física, Facultad de Ciencias, Campus Universitario Río San Pedro, Universidad de Cádiz, 11510 Puerto Real, Cádiz, Spain

Supporting Information

ABSTRACT: Mesoporous titania-silica composites that have photocatalytic activity have been synthesized by mixing ethoxysilane oligomers and titanium dioxide nanoparticles in the presence of a nonionic surfactant (*n*-octylamine). The resulting nanomaterials create effective adhesive and crack-free coatings for stone. These coatings give self-cleaning properties to stone and improve its mechanical resistance. In addition, the coating created has hydrophobic properties. For purposes of comparison, another two sets of photocatalytic materials have also been tested. The first of these has been obtained by an analogous synthesis in which *n*-octylamine is replaced by phosphoric acid; the second is a simple dispersion of titania nanoparticles in water. Both of these alternative materials produced coatings that crack and have poor adhesion on the stone tested; furthermore, they do not increase the mechanical resistance of the stone. These results confirm the valuable role played by *n*-octylamine in reducing the capillary pressure responsible for cracking, and in creating a mesoporous coating on the stone that enhances the self-cleaning properties, compared with the effect produced by the nanocomposite comprising similar particles embedded in a microporous silica matrix.

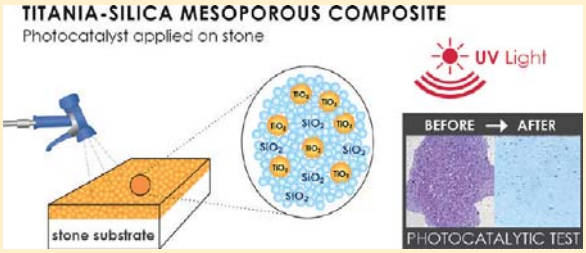

INTRODUCTION

Currently, titania is probably the most efficient common material with photocatalytic properties, very high stability, and very low cost.[1,2] Its unique combination of properties makes it very appropriate for many diverse applications in photochemical cells, self-cleaning materials, water purification, air cleaning, antitumor activity, and sterilization. Its development started with the description of an electrochemical photolysis phenomenon in 1972, by Honda and Fujishima.[3] Photons are absorbed by TiO_2, which generates electron−hole pairs, according to the equation:

$$TiO_2 + h\nu \leftrightarrow e^- + h^+ \quad (1)$$

In contact with water, free radicals are generated ($^{\bullet}O_2^-$ and $OH^{\bullet}$)

$$h^+ + H_2O_{ads} \leftrightarrow H^+_{ads} + OH^{\bullet}_{ads} \quad (2)$$

$$h^+ + OH^-_{ads} \leftrightarrow OH^{\bullet}_{ads} \quad (3)$$

These radicals are able to oxidize organic matter to water and carbon dioxide, leaving no other residue.[1]

In the case of self-cleaning applications, TiO_2 is deposited on the substrate as a thin film of thickness ranging from a few tens of nanometers to a few micrometers.[4] Titanium dioxide coatings can be prepared from titanium alkoxides through a simple sol−gel process, followed by a calcination treatment. This last operation at high temperature (>450 °C) promotes growth of rutile and anatase crystallites with photocatalytic activity and good adhesion to the substrate.[5,6] However, the most widely used photocatalysts are colloid TiO_2 nanoparticles, and more specifically Evonik Aeroxide TiO_2 P25.[7] Titania particles can also be subjected to calcination with particle sinterization and formation of covalent bonds between these nanoparticles with the object of producing materials that are considerably more robust and thermally stable than those prepared analogously from molecular precursors.[8]

The use of photocatalysts together with building materials began in the early 1990s. The versatility of TiO_2, which can serve both as a photocatalytic material and a structural material, has facilitated its application in exterior construction materials and interior furnishing materials, such as cement mortar, exterior tiles, paving blocks, glass, and PVC fabric.[9] With reference to titanium dioxide application on stones, only a few studies, with unsatisfactory results, are reported in the literature. Specifically, P25 particles dispersed in water have been applied on marble surfaces in order to prevent sulphation and bacterial activity;[10] these materials created a coating that cracked extensively on the marble surfaces under study. P25 slurry has also been applied on pumice stone for wastewater treatments; a significant decrease of photocatalytic efficiency was observed after 4 weeks, and this was mainly attributed to the elimination of TiO_2 from the stone surface.[11]

From these findings, our first objective has been to prepare a crack-free nanocomposite coating with good adherence to stone.

Received: August 4, 2011
Revised: September 14, 2011
Published: October 08, 2011

Such a coating should also give self-cleaning properties to the stone. The method for application of the coating must be simple, such as a spraying procedure, and the need for additional steps as calcination must be avoided because the coating will normally have to be applied in situ, on the external surface of a stone building. Moreover, high temperatures could damage the stone substrates. Our strategy is based on adding titanium dioxide colloidal particles to a silica oligomer in the presence of a surfactant. The target is to integrate TiO_2 particles into an effective silica matrix that is capable of adhering well to the stone. There are two reasons for adding surfactant: (1) to prevent cracking;[12−14] and (2) to enhance photocatalytic activity by creating a mesoporous nanocomposite.[4,15,16]

Synthesis strategies, in which mesoporous titanium dioxide films are obtained by using a surfactant as template have been widely reported in the literature.[17] Other strategies reported have employed surfactant-templated silica as a binding material for TiO_2 nanoparticles.[18,19] These particles are formed in situ within the porous matrix from a titanium precursor. The drawbacks associated with this synthesis are that the TiO_2 loading is quite low, and the capacity of the TiO_2 to crystallize into crystallites is severely limited by the low temperature of calcination permissible when using glass substrates.[20] Another approach is based on using preformed TiO_2 nanoparticles embedded inside surfactant-templated mesoporous films.[8,15,16,20−24] An ionic surfactant, such as Pluronic triblock copolymer or alkyl ammonium bromide, acts as a structure-directing agent to obtain mesoporous periodic structures. After the synthesis, the surfactant is removed by calcination or solid−liquid extraction.

In this work, we have synthesized a silica−titania nanocomposite starting from P25 titania particles mixed with a silica oligomer in the presence of *n*-octylamine. Our innovation with respect to the previously reported strategies is the employment of a nonionic surfactant to avoid the need for calcination or an extraction process. As we previously reported,[12−14] the surfactant can be removed very simply by drying under laboratory conditions. Silica interacts with the template by hydrogen-bonding; therefore, the removal of the surfactant in a neutral pathway must prove to be easier than the methods corresponding to the classic route involving electrostatic interactions between cationic surfactants and anionic inorganic. For the purposes of comparison, we also use another two different routes in this study. The three kinds of synthesis employed can be described as follows: (1) Aqueous dispersion of P25 particles; (2) Silica−titania nanocomposites are prepared from silica oligomer and titania nanoparticles in the presence of H_3PO_4; (3) Silica−titania nanocomposites are prepared from silica oligomer and P25 particles in the presence of *n*-octylamine.

For the three syntheses proposed, the proportion of titania to silica is varied from 0 to 2% w/v in each, in order to investigate its effect on the properties of the material. In the first part of the Results and Discussion section, we consider the characterization of the sol−gel properties of the materials synthesized. In the second part, we describe the application of these nanocomposites as a coating on a limestone surface, and evaluate their effectiveness for the following: (1) providing self-cleaning properties; (2) improving mechanical resistance of the coating; and (3) assuring its adherence to the substrate.

EXPERIMENTAL SECTION

Synthesis. The following reagents were used in the synthesis: (1) TES40 WN (Wacker Chemie AG, GmbH): according to the technical data sheet, this is an ethyl silicate providing approximately 41% of silica upon complete hydrolysis, and it contains many hydrolyzable ethoxy groups; (2) P25 (Evonik AEROXIDE TiO_2 P25): this material has an average primary particle size of 21 nm and a specific surface area (BET) of 50 ± 15 $m^2.g^{-1}$; (3) *n*-octylamine (Aldrich); 4. H_3PO_4 (Panreac). Three synthesis routes were followed:

(1) P25 particles were dispersed in distilled water under manual agitation.
(2) TES40 was mixed with P25 particles in the presence of H_3PO_4 under high-power ultrasonic agitation (125 $W \cdot cm^{-3}$); the proportion of H_3PO_4 to TES40 was 0.18% v/v. The total time of ultrasonic agitation was 10 min.
(3) TES40 was mixed with P25 particles in the presence of *n*-octylamine under the same agitation conditions. The proportion of *n*-octylamine to TES40 was 0.36% v/v.

Scheme 1. Summary Diagram of the Sols Tested

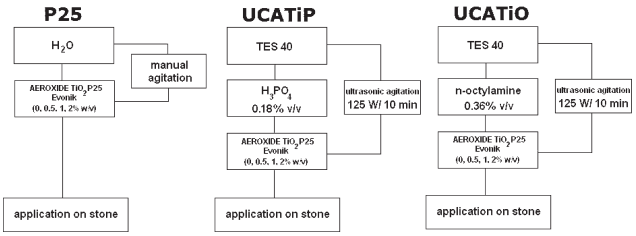

For each of the three synthesis routes, P25 particles were added to the starting sol (or water) in each of the following ratios: 0, 0.5, 1 and 2% w/v. The three formulations tested have been designated as follows: P25; UCATiP (TES40/P25/H_3PO_4); and UCATiO (TES40/P25/*n*-octylamine) via the procedure devised at the University of Cadiz. The numbers indicate the % w/v of P25 included in the material. Scheme 1 shows a summary diagram of the starting sols.

Immediately after the synthesis of the sols, their rheological properties were studied using a concentric cylinder viscosimeter (model DV-II+ with UL/Y adapter) from Brookfield. Experiments were performed at a constant temperature of 25 °C maintained by recirculated water from a thermostatic bath. A shear stress versus shear rate flow curve was generated. For comparison, the rheological properties of P25 aqueous dispersions were also evaluated.

Preparation and characterization of coatings. Coatings of the materials under study were obtained by deposition of 3 mL of sol on plastic Petri dishes with a diameter of 85 mm. Dishes were covered and maintained at laboratory conditions (relative humidity of 60% and temperature of 20 °C). Gel transition and spontaneous drying took place. The xerogels obtained were characterized after reaching constant weight.

Powdered coatings were used for X-ray diffraction (XRD), measured on a Bruker D8 advance diffractometer equipped with a secondary monochromator, Cu tube X-ray, using Cu kα radiation.

The pore volume, pore size distribution, and BET surface area of the coatings was characterized by Nitrogen Physisorption (Autosorb IQ from Quantachrome).

Transmission electron micrographs were obtained using high-angle annular dark field-scanning transmission electron microscopy (HAADF-STEM) by means of a JEOL 2010-FEG TEM/STEM electron microscope equipped with a JEOL HAADF detector.

The chemical bonds in the coatings under study were analyzed by Fourier Transformer Infrared Spectrophotometry (FTIR). The spectra were recorded in powder using a FTIR-8400S from Shimadzu (4 cm^{-1} resolution) in the region from 4000 to 600 cm^{-1}. Experiments were carried out in attenuated total reflection mode (ATR). In order to investigate surfactant removal as a function of time, FTIR spectra of the UCATiO gels were obtained, first immediately after the synthesis, and second after a period of 8 months had elapsed.

The materials were also visualized by Scanning Electron Microscopy (SEM) using a JEOL Quanta 200 Scanning Electron Microscope.

Application on Stone and Characterization. The stone selected for evaluating the effectiveness of the materials under study is a fossiliferous limestone with a homogeneous structure composed of a micritic matrix, containing recrystallized calcium carbonate grains, and skeletal fragments of mollusks, echinoderms, and foraminifera. Semiquantitative analysis by X-ray powder diffraction analysis enabled the mineralogical composition of stone to be identified; it is composed of calcite (98.5%) and α-quartz (1.5%). This stone was selected due to its whiteness, so the stains applied on its surface and self-cleaning effectiveness of the coatings under study could be checked more easily. For all of the experiments carried out, the stone samples were cut in the form of 5 × 5 × 2 cm slabs. For the water capillary absorption test, exceptionally, 5 cm-sided cubes were employed. The sols under study were applied by spraying onto the surfaces of the samples until saturation. The stone samples were then dried under laboratory conditions until reaching constant weight. Uptake of products and their corresponding dry matter were calculated. The samples corresponding to untreated stone and their treated counterparts were characterized by the procedures described below, after constant weight was reached.

A JEOL Quanta 200 scanning electron microscope (SEM) was used to visualize changes in the morphology of the stones after coating. Surface fragments of treated stone specimens and their untreated counterpart were visualized.

The adherence of the coating to the stone surface was evaluated by performing a peeling test using Scotch Magic tape (3M). The test was carried out according to previously reported methods.[25,26] The changes in stone surface morphology were visualized by SEM working in low-vacuum mode, and energy-dispersive X-ray spectroscopy (EDX) spectra were recorded in order to elucidate the variations in surface composition after the test.

The improvement in mechanical properties in treated stone was evaluated by using the drilling resistance measuring system (DRMS), by SINT Technology. Drill bits of 4.8 mm diameter were employed with a rotation speed of 200 rpm and penetration rate of 10 mm/min.

In order to investigate the hydrophobic behavior of the coatings under study, contact angles of the stone surfaces were measured using a commercial video-based, software-controlled contact angle analyzer, model OCA 15plus, from Dataphysics Instruments.

Changes in water absorption after treatments were evaluated by applying a test of water absorption by capillarity, as recommended in UNE-EN 1925.[27] Total water uptake values (TWU) obtained after 48 h were determined.

We also evaluated the possible disadvantage of these materials associated with changes in stone color induced by the treatments. This effect was determined using a solid reflection spectrophotometer, Colorflex model, from Hunterlab. The conditions used were as follows: illuminant D65 and observer 2°. CIELa*b* color space was used and variations in color were evaluated using the parameter: total color difference (ΔE^*).[28]

The effectiveness of the materials under study as self-cleaning coatings for stone surfaces was evaluated by using a test adapted from the literature.[29,30] First, 1 mL of a solution of 1 mM methylene blue (Panreac) in ethanol was deposited on treated stone specimens and their untreated counterparts. Next, stone samples were irradiated with UV light working at 365 nm in a Vilber Lourmat CN15.CL chamber with 2 tubes of 15 W. The distance between the samples and the tubes was approximately 20 cm. Color variations, recorded as a function of irradiation time, were determined by using the same procedure described above. The parameter total color difference (ΔE^*) was again evaluated.[28]

Table 1. Viscosity Values (Measured at 25° C), Textural Parameters Obtained from the Isotherms and the BJH Method for the Nanocomposites under Study

sample	viscosity (mPa·s)	S_{total} (m^2/g)	V_{pore} (cm^3/g)	pore size (nm)
P25-0.5	2.70	59	0.39	28
P25-1	2.73			
P25-2	2.75			
UCATiP-0	5.25	267	0.22	3.8
UCATiP-0.5	5.32	220	0.23	3.8
UCATiP-1	5.45	259	0.23	3.8
UCATiP-2	5.50	249	0.18	3.8
UCATIO-0	5.30	231	0.39	6.3
UCATiO-0.5	5.54	255	0.31	7.6
UCATiO-1	5.68	180	0.69	13.4
UCATiO-2	5.82	220	0.59	13.0

RESULTS AND DISCUSSION

Coatings Characterization. Prior to the preparation of the coatings, a rheological study of the sols was carried out. Although a shear-thinning behavior for aqueous titanium dioxide dispersions is commonly reported in the literature,[31] we observed a Newtonian behavior for the three concentrations of P25 aqueous dispersion studied, at the shear range evaluated. We explain this finding in terms of the low particle concentration in the dispersions under study. These viscosity data were obtained immediately after stirring the dispersions. After a few hours, the P25 particles tend to aggregate, and flocculation occurs for all of the concentrations studied. This demonstrates that the P25 aqueous dispersions prepared are not stable. UCATiP and UCATiO sols also showed Newtonian behavior at the shear range evaluated. The viscosity was calculated as the slope of the shear rate vs shear stress curve. In all of the cases, the linear regression coefficients were above 0.99. Viscosity values obtained are listed in Table 1. In the case of the P25 dispersions, the viscosity increased only slightly when the particle concentration was increased. In the case of the silica−titania sols under study, the addition of P25 promoted a more significant increase in viscosity, following a linear trend. In comparison with the commercial products, the values of the UCA sols synthesized in this study were only slightly higher than those corresponding to commercial sols. Specifically, we determined the viscosity for one of the most

popular commercial consolidants, Tegovakon V100 from Evonik; the viscosity of this solvent-free product was 4.48 mPa·s at 25 °C. Thus, we think these sols must penetrate into the stone in a similar way to that of the commercial sols. This is a key factor for achieving a consolidant effect on the stone.

Sol−gel transition of all the UCATiP and UCATiO sols deposited on plastic dishes occurred overnight, producing homogeneous nanocomposite gels. When P25 is mixed with TES40, we find that one of two different processes may occur: (1) flocculation of the P25 particles and subsequent creation of two different phases; or (2) the P25 particles are stable in the sol during the hydrolysis of TES40 and the condensation of silanols, and thus titania particles are integrated within the gel network. Obviously, the homogeneity of gels obtained indicates that stabilization of the particles is achieved by means of the two routes investigated in this work. We think the particles exhibit stability during the sol−gel transition because of an electrostatic repulsion phenomena, induced by pH-changes produced by H_3PO_4 or *n*-octylamine. As previously discussed,[32,33] the interaction between charged particles is well described by the DVLO theory, which is based on an algebraic sum of the attractive van der Waals and the repulsive double layer forces. Since the isoelectric point of the P25 particles is 6.5 for water, their isoelectric point in the sols prepared in our laboratory must be fairly close to this value. Therefore, adjusting the pH to higher or lower values by acid or basic addition to the sol must increase electrostatic repulsions and, subsequently, P25 dispersion stability must be enhanced. Electrostatic stabilization of P25 particles in polar organic solvents has previously been obtained by Kosmulski et al.[33] by adding an acid such as phosphoric acid and a base like triethylamine. Furthermore, it should be noted that H_3PO_4 works as an acid catalyst during sol−gel transition and *n*-octylamine acts as a basic catalyst in the same way. Thus, sol−gel transition took place in a maximum time of 24 h for the two series of sols tested.

We previously investigated other proportions of *n*-octylamine ranging from 0.016 to 1.8% v/v. We chose 0.36% v/v because it is the minimum concentration at which a stable titania particle dispersion can be obtained during the sol−gel transition time (24 h). Lower concentrations of surfactant resulted in phase separation. In addition, these sols with lower *n*-octylamine content do not gel spontaneously. This finding corroborates the role played by the surfactant as basic catalyst. Regarding the higher concentrations of the surfactant, they were not adopted because they gradually decreased the gel time. For the highest concentrations tested, the gel transition occurred immediately after synthesis. This short gel time is not sufficient for the sol to be applied to the substrate.

The X-ray patterns of the powdered form of the coatings under study are given in Figure 1. All of the materials show the typical amorphous silica pattern without any detectable ordered structure. We have previously obtained[34] similar patterns for silica gels synthesized from TEOS and *n*-octylamine. This confirms that our synthesis strategy does not promote an ordered pore structure, which is typical of most materials synthesized via a surfactant template. As previously reported,[23] the silica/titania films become an ordered mesostructure at higher drying temperatures. Thus, we assume that our drying at ambient temperature cannot produce an ordered silica structure.

We also observe that the X-ray patterns obtained show peaks previously reported as a pure anatase structure.[22,35] Specifically, the peaks assigned to anatase-type titania at around 25°, 38°, and 48° were observed.[23] This demonstrates the loading of TiO_2 particles in the coatings under study. In addition, as reported in previous papers,[8,35] this verifies that the TiO_2 particles in the nanocomposites prepared in our laboratory exist as a separate domain embedded within the silica domains. As would be expected, these peaks in the patterns corresponding to the material with the lowest content of TiO_2 particles are difficult to appreciate, whereas their resolution and sharpness improve at higher TiO_2 contents.

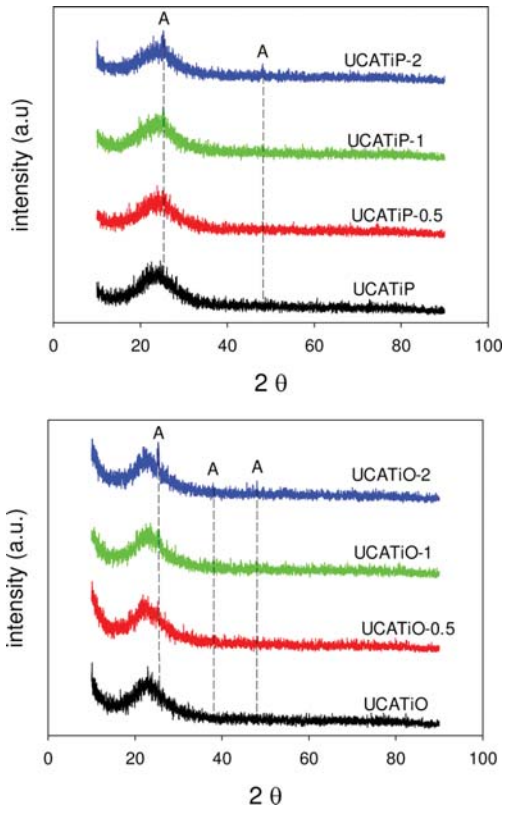

Figure 1. XRD patterns for the nanocomposite coatings under study.

Nitrogen adsorption−desorption isotherms corresponding to the coatings are shown in Figure 2, and the textural data obtained are given in Table 1. P25, which was also characterized for comparative purposes (see isotherm in Supporting Information), presents a type IV isotherm with an H1 hysteresis loop, as expected for an agglomerate of TiO_2 particles.[36] In the case of UCATiP materials, type I isotherms are observed, corresponding to microporous materials. These isotherms show a slight hysteresis typical of mesoporous materials. This profile is characteristic of materials consisting of a mesoporous network with a pore size close to microporous values.[36]

Regarding the materials designated UCATiO, the isotherms are type IV, showing an H1 hysteresis loop with parallel and nearly vertical branches. This loop is more clearly observed for materials with the highest TiO_2 content (1 and 2% w/v). As reported for P25,[36] this kind of hysteresis is attributed to materials consisting of agglomerated particles or compacted clusters of spherical particles arranged in a uniform way. These isotherm profiles therefore suggest that UCATiO gels are composed of a network of silica balls and the titania particles are integrated within this network. We have previously obtained[34] similar morphologies, consisting of a regular network

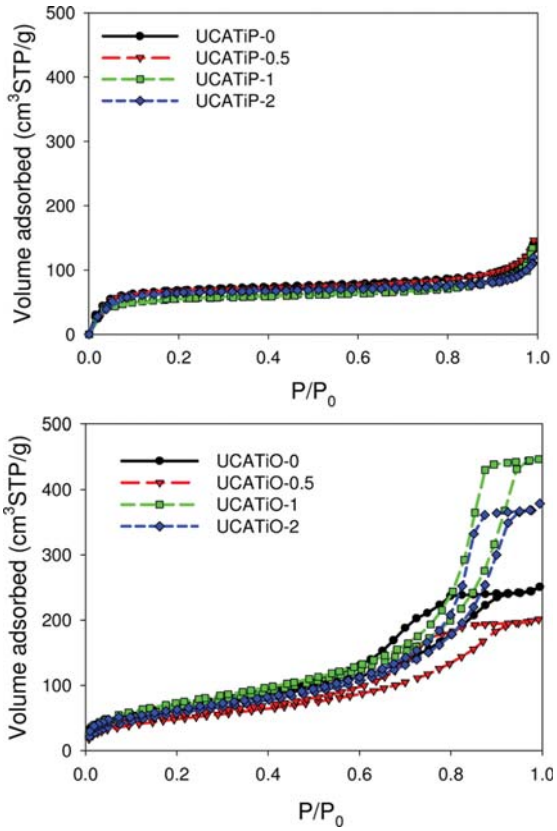

Figure 2. Nitrogen adsorption−desorption isotherms for the nanocomposite coatings under study.

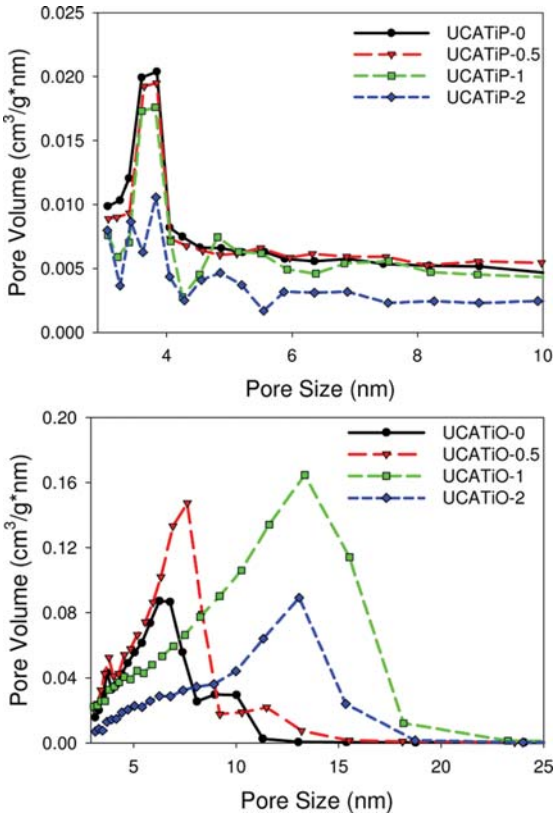

Figure 3. BJH pore size distribution for the nanocomposite coatings under study.

of uniform silica spheres for gels obtained from TEOS and *n*-octylamine.

The pore-size distribution (Figure 3) was determined using the Barret−Joyner−Halenda (BJH) method.[37] Pore volume (see Table 1) and pore size were significantly higher when the synthesis occurs in the presence of *n*-octylamine. Pore volume detected in the mesoporous range for UCATiP materials were 1 order of magnitude less than that obtained for the UCATiO coatings. As we demonstrated in our previous papers,[12−14,34] this feature indicates the role played by the surfactant: it coarsens the pores network and this subsequently reduces the capillary pressure responsible for cracking during the drying of the gel.

Concerning the effect of TiO_2 content on the pore structure of the coatings, we do not observe any significant differences for UCATiP materials. It is thought that the low pore volume detected at 3 nm can be attributed to the silica material in which the TiO_2 particles are embedded. In the case of the UCATiO materials, we observe a completely different behavior. The UCATiO gel without TiO_2 content and that with the lowest proportion of TiO_2 (0 and 0.5% w/v) presents pores of size around 6 nm, which are attributed to the silica network. As we have previously reported, the presence of surfactant promotes the coarsening of the gel network, increasing the size and uniformity of the pore network, as corroborated by nitrogen adsorption test data. The formation of this coarser network composed of polymeric balls is due to the *n*-octylamine. We assume that the pores detected correspond to the voids between the silica particles. For materials with the highest TiO_2 content, the pore size of the silica/titania composite is greater, at 13 nm. Since P25 particles present a mean pore size of 28 nm (see Table 1; pore size distribution is included as Supporting Information), a value taken to correspond to interparticulate space, we speculate that titania particles are intercalated in the interparticle spaces formed between the silica balls, created by the surfactant. Since pore size doubles when titania is integrated in the silica network, we believe that the silica particles are smaller than the P25 particles. Thus, P25 integration in the silica network produces greater heterogeneity in the pore size of the network. Regarding BET surface area (Table 1), although the pore volume is higher for the UCATiO materials, the two series show similar surface area values because the pore size of UCATiO composites is significantly higher than that corresponding to UCATiP materials.

These findings were supported by the transmission electron micrographs of the coatings. Figure 4 shows micrographs corresponding to UCATiP and UCATiO materials with the highest TiO_2 content. The HAADF-STEM micrograph of the UCATiP coating shows a material composed of individual TiO_2 particles (of around 20 nm size) and some aggregates (of 30−40 nm size) of titania particles embedded in a dense silica matrix, whereas the micrograph corresponding to UCATiO clearly shows a gel network composed of individual titania and silica particles. Uchiyama et al.[22] obtained a similar morphology for a coating prepared from titania particles with a smaller diameter (of around 7 nm) than those we employed— and a mesoporous structure; their coating was synthesized through the combination of a surfactant and a siliceous monomer. Yamauchi et al.[15,16] have also obtained a similar nanocomposite of P25 and silica particles.

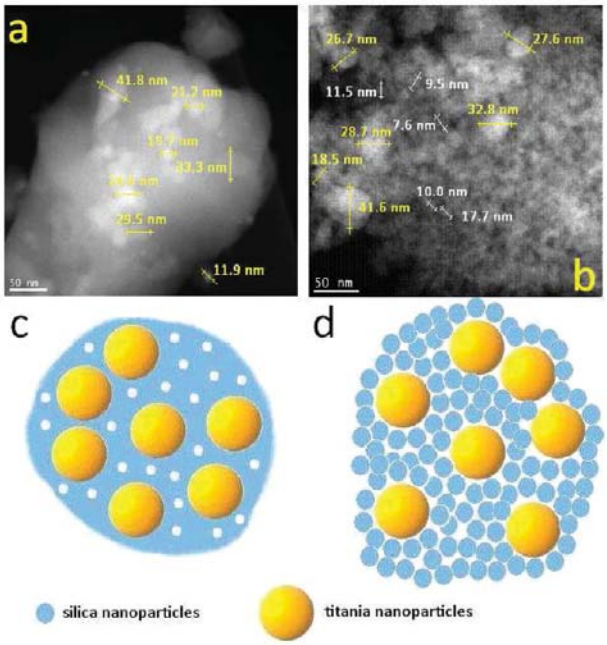

Figure 4. HAADF-STEM images of (a) UCATiP-2; and (b) UCATiO-2 coatings. Parts (c) and (d) are schematic models of these nanocomposites.

Our micrographs provide evidence of the presence of titania particles with similar size to those observed in the UCATiP nanocomposite. Concerning the silica network, an aggregation of mesoporous particles with a slightly lower diameter (7−15 nm) than the titania particles, can be observed. These findings confirm the greater pore size of the network for the coating materials with higher TiO_2 content, demonstrated by nitrogen physisorption. As is obvious, larger particles produce larger pores in the network. A schematic model of the structures of the composites is also included in Figure 4.

FTIR spectra of the coatings under study are shown in Figure 5. For comparative purposes, the spectrum of TES40 has been included as Supporting Information. All of the materials present the typical silica peaks.[12,38,39] Specifically, the bands located at 800 and 1080 cm^{-1} are attributed to Si−O−Si bending; the band at 960 cm^{-1} is attributed to Si−OH stretching; and the broad band in the 3400 cm^{-1} range is attributed to Si−OH groups with absorbed molecular water. This band may also contain the contribution of absorbed molecular water on Ti−OH from the surface of TiO_2 particles. In addition, another band associated with ethoxy groups of the silica precursor is also observed: the band located at 1300 cm^{-1} attributed to CH_2 twisting.[39] This last band confirms that all the ethoxy groups are hydrolyzed immediately after the synthesis. Comparison between the two sets of gel under study shows that UCATiO gels present sharper Si−O−Si peaks than UCATiP gels. This difference can be attributed to higher condensation of silanols in a ramified structure obtained through the effect of *n*-octylamine.

The possible presence of residual surfactant in the UCATiO material was investigated by carrying out FTIR assays at two time intervals (the first immediately after synthesis and another after 8 months). In the spectra obtained immediately after synthesis, we can observe a peak at 1400 cm^{-1}, which is attributed to amine C−N[12,13] stretching, from the surfactant. In addition, in the

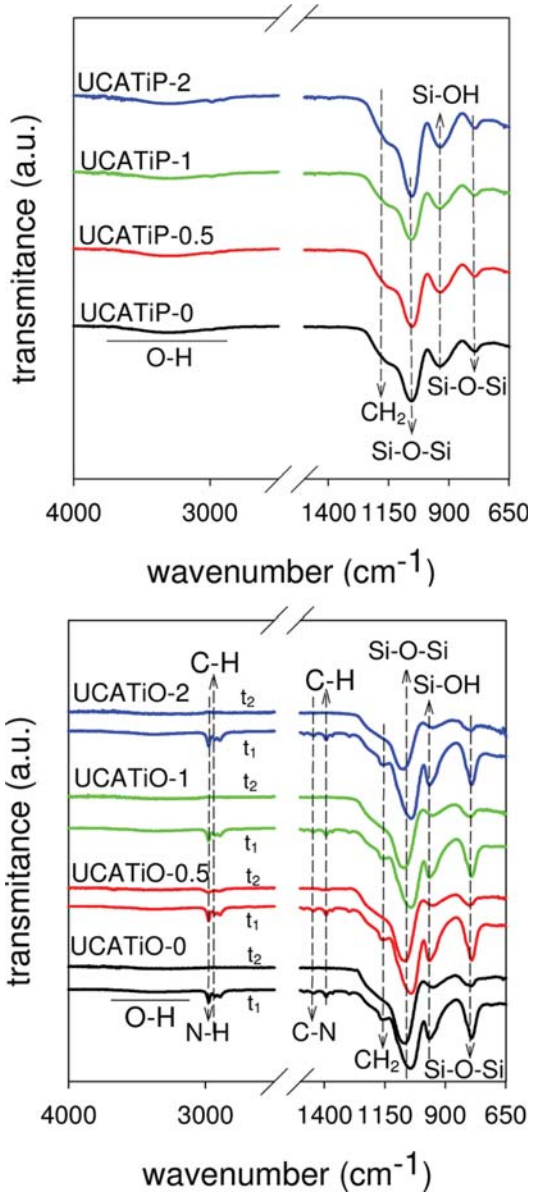

Figure 5. FTIR spectra for the coatings under study. UCATiO spectra were recorded at two time points: (t_1: immediately after the synthesis; t_2: after 8 months had elapsed).

spectra for this time, two bands at 2883 and 1430 cm^{-1} can be attributed to stretching and bending, respectively, of the C−H bond.

Finally, the peak at 2930 cm^{-1} corresponds to N−H stretching.[12,13] These peaks have almost disappeared after 8 months. From these results it can be concluded that n-octylamine is removed by simple exposure to laboratory conditions.

Moreover, the band at 1300 cm^{-1} attributed to ethoxy groups is significantly reduced after 8 months, confirming the hydrolysis and subsequent condensation of silica oligomers. However, the presence of a weak shoulder confirms that a small proportion of nonhydrolyzed ethoxy groups is present in the coatings under study.

Regarding the peaks associated with titania, it is often reported[40] that bands observed in the range 900−1000 cm^{-1} may be associated with Ti−OH and Si−O−Ti species. These bands could appear in our spectra due to co-condensation

between silica oligomer and titania particles. However, they are not visible because these bands are probably obscured by the peak attributed to Si−OH located at the same wavenumber.

Figure 6 shows the SEM micrographs of the coatings under study. We can observe significant differences in the morphology of the two sets of nanocomposites studied. The UCATiO materials form a homogeneous and continuous gel coating whereas the UCATiP materials create discontinuous films of aggregates. These features provide evidence supporting that from the FTIR spectra obtained. As previously reported, the UCATiO gels present sharper Si−O−Si peaks than the UCATiP gels due their higher degree of condensation in a cross-linked structure. The SEM micrographs also contribute to corroborating the structure model presented in Figure 4, since silica aggregates observed in UCATiP images show sizes of around 300−400 nm, which are similar to the size of the silica aggregates measured by HAADF-STEM for UCATiP2 (see also Figure 4).

Application on Stone and Characterization. The effectiveness of UCATiP and UCATiO nanocomposites was investigated on the surface of a limestone. For purposes of comparison, the effectiveness of aqueous dispersions of P25 at the same TiO_2 concentrations was also investigated. Uptake of the materials under study and dry matter are shown in Table 2.

The uptake of the P25 aqueous dispersion was slightly higher than that corresponding to the gel coatings because its viscosity is lower. However, dry matter values were significantly lower for P25 than for UCATiO and UCATiP, since the P25 dispersion only creates a deposit of particles on the surface of stone, whereas the two coating materials penetrate into the stone pore structure. Higher content of TiO_2 particles does not significantly modify the values for dry matter obtained. Comparing the two series of gels, the dry matter for the UCATiO nanocomposites was slightly higher.

Figure 7 shows SEM micrographs of stone specimens treated with the materials under study. The P25 and UCATiP materials create a dense and extensively cracked coating on the stone surface. In the case of the UCATiO materials, crack-free, homogeneous, and coarser coatings on the stone surface are observed.

This demonstrates that *n*-octylamine efficiently reduces the capillary pressure, which is the factor responsible for cracking, by coarsening the gel network pore size. Moreover, *n*-octylamine also reduces the surface tension of the starting sol, which also contributes to reducing the capillary pressure. Since one significant drawback of P25 applied on stone has been associated with a reduction in photocatalytic efficiency during long-term use, due to the elimination of TiO_2 from the stone surface,[11] we have investigated the degree of adhesion of these coatings synthesized in our laboratory on stone, by performing a peeling test adapted by the literature. Figure 8 shows the micrographs obtained by SEM and the EDX analyses carried out on tested and nontested areas. As expected, a gradual increase of titanium content is observed as P25 content is raised in the coatings analyzed. Cracks in the coatings are not observed due the different observation scale. In P25 coatings, an almost complete removal of the titania coating after the peeling test can be observed. This was confirmed by EDX analysis, since the high titanium peaks are completely removed for P25-0.5 and P25-1 and significantly reduced for P25-2, after the test.

The UCATiP coatings show similar adhesion performance than the P25 ones, as confirmed by the absent titanium peaks

Table 2. Properties of the Treated Stone Specimens and the Untreated Counterpart

sample	untreated	P25-0.5	P25-1	P25-2
uptake (%w/w)		2.09 ± 0.44	2.30 ± 0.59	2.55 ± 0.54
dry matter (%w/w)		0.04 ± 0.02	0.05 ± 0.03	0.05 ± 0.02
contact angle (deg)	61 ± 9	70 ± 12	65 ± 16	23 ± 4
TWU (%w/w)	2.72 ± 0.08			
ΔE^a		0.66 ± 0.21	1.57 ± 0.85	1.59 ± 0.83
sample	UCATiP-0	UCATiP-0.5	UCATiP-1	UCATiP-2
uptake (%w/w)	1.31 ± 0.29	1.43 ± 0.39	1.28 ± 0.24	1.15 ± 0.36
dry matter (%w/w)	0.89 ± 0.17	1.13 ± 0.31	1.07 ± 0.20	0.93 ± 0.30
contact angle (deg)	93 ± 2	92 ± 6	98 ± 2	96 ± 6
TWU (%w/w)	0.08 ± 0.01	0.08 ± 0.01	0.07 ± 0.01	0.09 ± 0.01
ΔE^a	3.66 ± 0.49	2.68 ± 0.31	2.27 ± 0.31	1.72 ± 0.25
sample	UCATiO-0	UCATiO-0.5	UCATiO-1	UCATiO-2
uptake (%w/w)	1.43 ± 0.09	2.48 ± 0.32	1.58 ± 0.19	1.70 ± 0.29
dry matter (%w/w)	1.05 ± 0.06	1.78 ± 0.23	1.15 ± 0.14	1.31 ± 0.23
contact angle (deg)	121 ± 1	118 ± 6	101 ± 6	88 ± 3
TWU (%w/w)	0.10 ± 0.00	0.09 ± 0.0	0.11 ± 0.00	0.10 ± 0.02
ΔE^a	5.92 ± 1.24	5.34 ± 0.32	4.40 ± 0.19	3.51 ± 0.40

[a] Data correspond to average values. Standard deviations are also included.

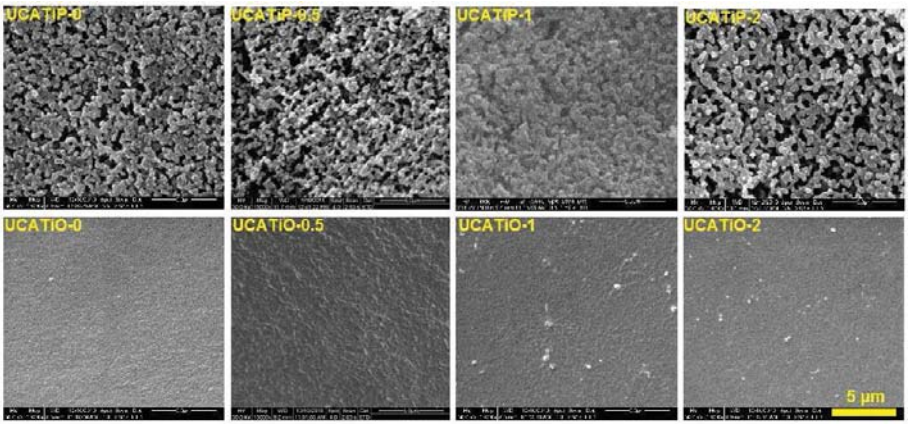

Figure 6. SEM micrographs of the nanocomposite coatings under study.

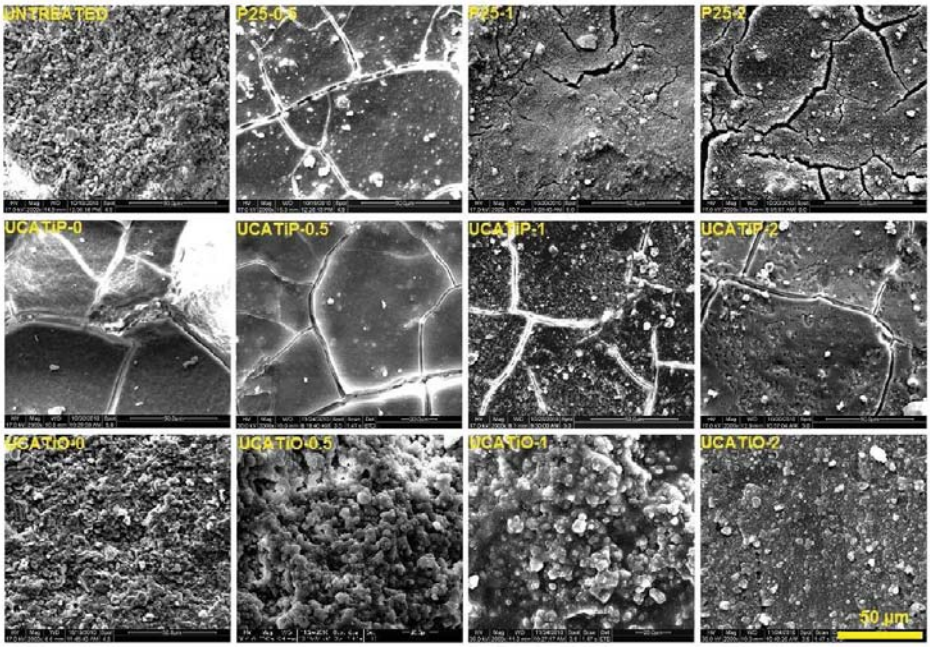

Figure 7. Scanning electron microscopy micrographs of the coatings on the limestone under study.

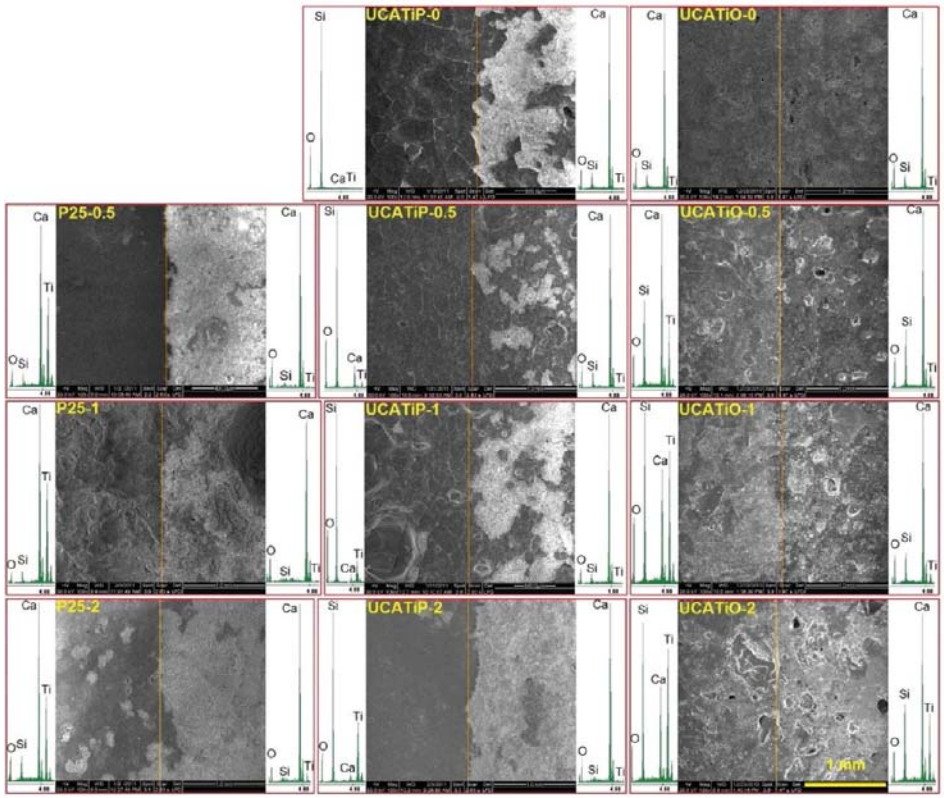

Figure 8. Scanning electron microscopy micrographs of the limestone under study after the peeling test. On the left side of each micrograph, nontested surface is presented, together with the corresponding EDX spectrum. On the right side, the corresponding tested surface and spectrum are presented.

shown by the coatings after the test. However, a significant reduction of TiO_2 content was observed for all the treatments tested. Concerning the calcium content (from limestone), we observe a significant increase in this peak after the peeling test, which confirms that the coating has been largely eliminated from the surface stone. For P25, an increased calcium peak is not

detected because the particles do not create a coating on the surface, and so components of the stone are also detected before the test.

In the case of the UCATiO coatings, differences in morphology between treated and nontreated zones are more difficult to observe. Regarding the EDX results, no significant changes were detected after the tests. These findings confirm that TiO_2 particles have been integrated into the silica matrix, which has been capable of adhering firmly to the stone. We can thus conclude that the inclusion of the photocatalyst in a silica coating is an interesting solution for keeping particles adhered well to the surface, providing long-term wear resistance.

We also investigated whether the mechanical resistance of a stone surface is improved after application of the coatings; this was done by measuring the drilling resistance of the untreated limestone and its treated counterparts. The results obtained are shown in Figure 9.

As expected, P25 deposited on stone does not produce any increased mechanical resistance. Nor do the UCATiP coatings increase the stone's resistance, either. However, in the case of the UCATiO materials, we observe a clear increase in drilling resistance to a depth of 4 mm. The ineffectiveness of the UCATiP coatings for consolidating stone is thought to be associated with the extensive cracking that occurs and with their poor adherence to the stone. In the case of the UCATiO materials, it is obvious that they create a homogeneous, crack-free coating that adheres well to the limestone. Moreover, the results confirm that octylamine is playing a valuable role in enhancing their effectiveness, since silicon-based products are known to be ineffective as consolidants on pure carbonate stones.[41] In a previous study, we found increased drilling resistance for the same limestone by using a silica/PDMS hybrid coating material obtained in presence of *n*-octylamine.[14]

Since the water is the main vehicle carrying the agents of decay, such as soluble salts, microorganisms, etc., that attack building stones, any hydrophilicity induced in the coatings by the P25 particles is undesirable. Therefore, we have also measured water droplet static contact angles (CA) on the surface of stone samples treated with the coatings under study and the untreated counterpart. Results obtained are given in Table 2. As expected, the untreated stone surface shows a hydrophilic behavior with a static CA of 60°. Stone surfaces treated with the P25 dispersions at lower concentrations show a similar droplet CA value as the untreated surface, whereas the P25 dispersion with the highest TiO_2 content induced a significant reduction in the CA value. This finding suggests that, in dispersions with lower concentrations, particles do not completely cover the stone surface and thus, the static CA of the surface is not modified. The low contact angle obtained for the P25-2 coating corroborates the hydrophilic character of P25. In the case of the UCATiP and UCATiO coatings, the hydrophobic behavior may be associated to the presence of some nonhydrolyzed ethoxy groups in the gel coatings under study. Contact angles obtained are slightly lower for the UCATiP coatings than those for UCATiO. We think that discontinuity observed for these coatings could be responsible for this slight reduction. In the case of the UCATiO materials, coatings show a clear hydrophobic behavior, with a linear decrease as the content of TiO_2 particles increases.

Regarding changes observed in contact angle values as TiO_2 content is increased, in the case of UCATiO materials, coatings show the expected linear decrease as the content of titania increases. However, UCATiP contact angles remain constant.

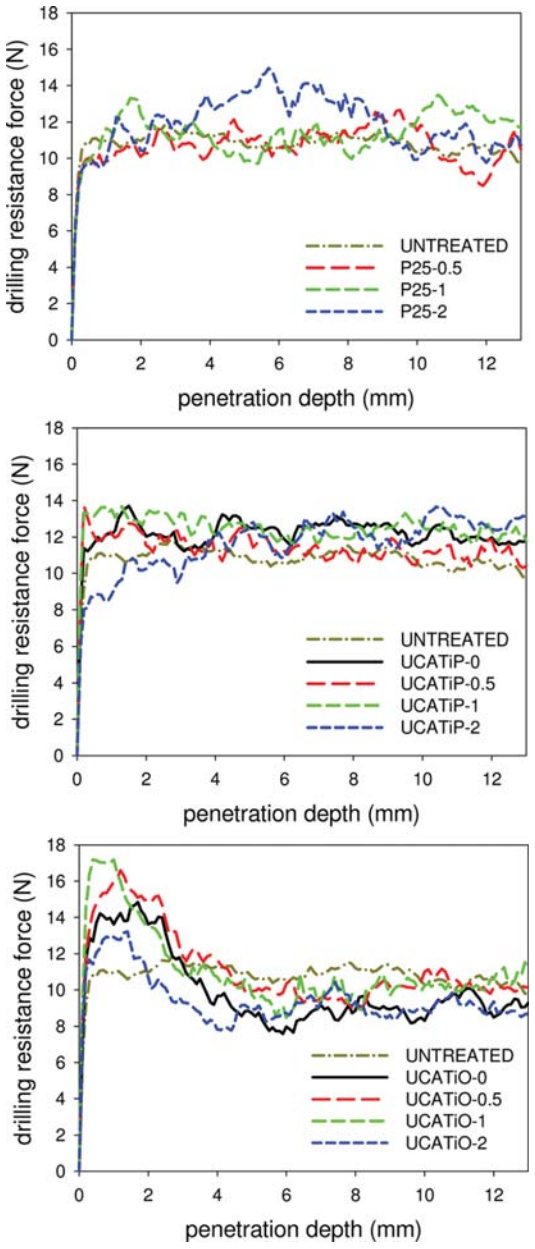

Figure 9. Drilling resistance measurements for the treated limestone under study.

As previously discussed, the UCATiP coatings are composed of titania particles integrated in a dense silica matrix with a low porosity. Thus, the titania particles are shielded by the silica matrix and, consequently, the accessibility of water to the titania is difficult. A similar discussion can be read in the paper by Horiuchi et al.[42] These authors stated that the enhancement of porosity in silica−titania thin films by the employement of structure-directing agents promotes the improvement of hydrophilic properties because of a capillary penetration effect.

We have tested the ability of the coatings to prevent water penetration into the stone, by applying a test of water absorption by capillarity. Total water uptake values (TWU) obtained after 48 h are shown in Table 2. The results confirm the hydrophobic behavior of the UCATiP and UCATiO coatings, since the uptake

values obtained are practically zero and significantly lower than that for the untreated counterpart. Moreover, no significant differences were found for coatings with differing TiO_2 content. These findings demonstrate that the inclusion of a small content of hydrophilic particles, i.e., P25, in a silica coating matrix does not induce capillary water absorption.

Total color difference values (ΔE^*) of the stone after the treatments are shown in Table 2. The P25 dispersions and UCATiP produced small values of ΔE^*, below the perception threshold ($\Delta E^*<3$).[28] The UCATiO coatings produced slightly greater changes in color, which were progressively reduced as TiO_2 content increases. We associate the color change with the effect due to *n*-octylamine, which imparts a slightly yellowish color to the white limestone tested. This disadvantage is progressively reduced as P25 content is raised, since the titania particles have a whitening effect.

Lastly and most importantly, we have investigated the self-cleaning properties of the coatings on the limestone tested by carrying out a photodegradation test of stains deposited previously on the stone surface. Methylene blue (MB) was used as the staining agent. The evolution of total color differences under UV light with the time was recorded and results are shown in Figure 10 for the three sets of coatings under study. Of all of the materials tested, the P25 dispersions present the most rapid bleaching of the MB stains. In the first 6 h, the stain is almost completely degraded (88% of the total change is observed after this period of time has elapsed). Comparing the performance of the various P25 dispersions, a modest increase in self-cleaning activity is found in line with higher TiO_2 content; the final ΔE^* values are 15, 9, and 7 for P25 content of 0.5, 1 and 2%, respectively.

In the case of the untreated stone, the final ΔE^* value reached is 30, after more than 800 h of exposure, corresponding to a "natural" reduction of 25%. MB bleaching under visible/UV light has been reported previously and this bleaching has been associated with a weak absorption of light undergone by the dye in the 350−520 nm range.[43,44] Thus, we think the degradation of MB on untreated limestone is induced by the light absorbed during its long exposure (around 800 h) to the UV lamp.

For the two series of nanocomposites materials, the MB degradation rate is slower than that presented by the P25 dispersions. This lower degradation rate can be explained by the low TiO_2 content in all the coatings prepared (a maximum of 2%). For all of the materials synthesized, two different rates of change can be clearly distinguished in the degradation profiles. Very rapid MB bleaching occurs in the first 7−12 h, accounting for around 80% of the total color variation recorded. Next, a slower rate of degradation is observed over the longer term. Again, small differences in ΔE^* values are found for the differing TiO_2 concentrations tested. These differences are appreciated mainly in the initial rate of degradation in which the coatings with the higher P25 content (1% and 2%) show larger falls in ΔE^* value. Considering the performance of the nanocomposites coatings prepared without TiO_2 particles, we also observe a bleaching effect under UV exposure. A degradation profile similar to that corresponding to the slower, second-stage rate for titania/silica composites is now observed.

The two findings reported above clearly confirm that the photocatalytic action of the titania particles produces most of the total degradation effect on the stain in the first few hours of exposure (the first part of the curve). We think that the second stage with a much slower rate of degradation may be caused by

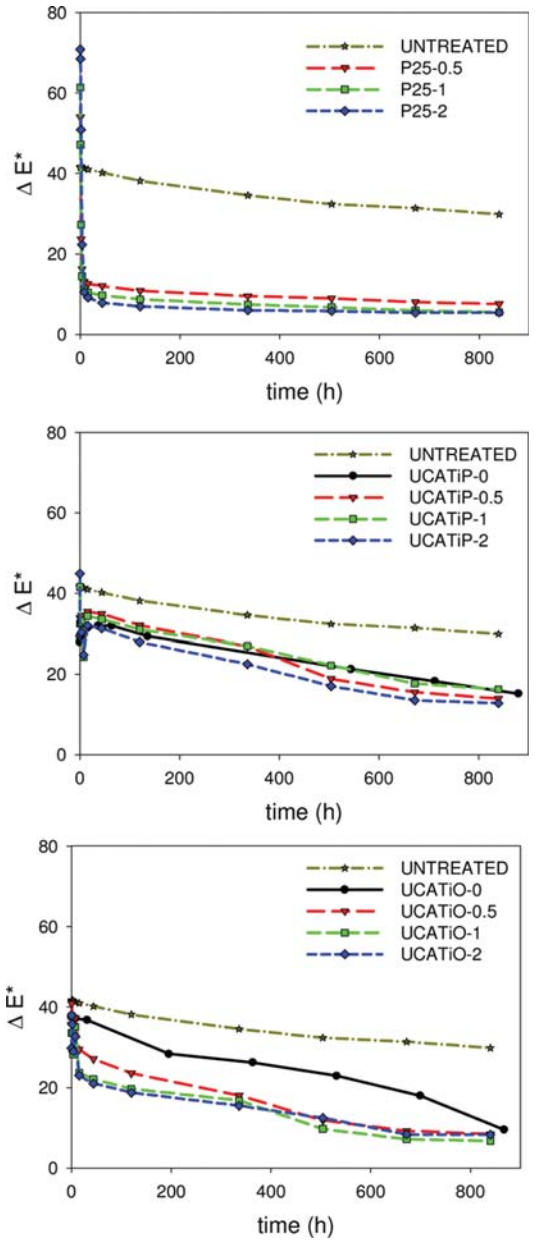

Figure 10. Evolution of total color difference (for methylene blue stains) on treated and untreated samples of limestone.

the silica/titania coating reducing the capacity of the MB to penetrate into the limestone pore structure. The greater the proportion of MB on the surface of the coated limestone, the greater the proportional degradation by the bleaching effect of the UV light absorbed. Variations found in the degradation kinetics between the UCATiP-0 and UCATiO-0 coatings corroborate our hypothesis, since the material with lower porosity (UCATiP-0), which was subsequently shown to be associated with lower penetration of MB into the pore structure of the limestone, induces a more rapid degradation than the UCATiO-0 coating.

Comparing the performance of the two series of gels, we found that the UCATiO gels show greater self-cleaning activity, since their rate of degradation in the rapid first stage is slightly higher and the final ΔE^* values produced in the longer term are lower.

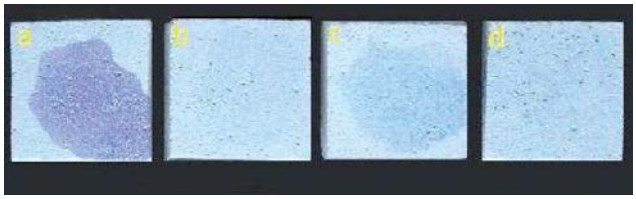

Figure 11. Photographs after the self-cleaning test of the surfaces of stone samples treated with the coatings under study, with 2% w/v TiO_2 content. (a) Untreated stone; (b) Stone treated with P25-2; (c) Stone treated with UCATiP-2; (d) Stone treated with UCATiO-2. The samples were previously stained with Methylene Blue and then irradiated with UV light (λ = 365 nm) for more than 800 h.

The UCATiP nanocomposites present final ΔE^* values of ~15, whereas the UCATiO materials show ΔE^* values of ~7. This last final value is similar to that obtained with the P25 dispersions

Figure 11 shows photographs of the stone surfaces under study after completion of the test. The samples illustrated are the stained limestone surfaces untreated and treated with the three different coatings with the highest TiO_2 content (2%). Photographs corresponding to the other coatings evaluated are shown as Supporting Information. It can be observed that the stone surface treated with the UCATiP-2 coating shows the lowest degradation of the MB stain. The degree of change in color induced by the P25-2 and UCATiO-2 nanocomposite coatings is similar.

The greater self-cleaning effect produced by the UCATiO coatings is explained by their higher porosity and the larger pore size of the gel network. As previous authors have reported,[15,16] the photocatalytic degradation of MB is clearly enhanced by the addition of TiO_2 particles to a silica mesoporous structure, in comparison with the effect observed when the particles are integrated in a dense microporous matrix. This enhancement effect was explained by these authors in terms of the increased BET surface area, which accelerates the diffusion of MB toward the reaction sites (i.e., toward the titania particles). The authors of this study have also reported previously that the presence of mesopores also assists rapid diffusion. As discussed earlier in this work, the UCATiO coatings create a pore structure in the gel network completely different from that corresponding to the UCATiP materials. According to the model proposed on the basis of the HAADF-STEM images (Figure 4), the UCATiO gels create a field of silica and titania particles with numerous voids between particles, making the sites with photocatalytic activity, the titania particles, much more accessible for the MB molecules. In the case of the UCATiP material, however, a dense and microporous silica gel with titania particles embedded is clearly observed; in this material, the photocatalytic sites will now be less accessible to the MB.

From these results, we conclude that the addition of titania particles to a silica mesoporous structure created using a surfactant as template creates a material with effective photocatalytic activity, and the MB bleaching obtained is similar to that obtained by the P25 aqueous dispersion. As a final note, it can be confirmed that this new nanocomposite coating developed in our laboratory will become available as a commercial product under an exploitation patent.[45]

CONCLUSIONS

An effective new synthesis method has been developed for producing titania-silica nanocomposite coatings for stone conservation with self-cleaning application. Composite coatings are prepared by dispersion of TiO_2 nanoparticles in a mesoporous silica matrix in the presence of a nonionic surfactant (*n*-octylamine). This surfactant acts in several distinctive ways in the synthesis: (1) it prevents the unwanted aggregation of titania particles in the starting sol; (2) it acts as a basic catalyst of the sol−gel transition; and (3) by serving as a template, it increases the pore size of the final material, thus preventing unwanted cracking. Moreover, the surfactant can be removed very simply by ambient air drying; therefore the user will be able to apply the starting sol, in situ, on the stone of the building or structure to be protected. Sol−gel transition occurs spontaneously, producing an effective nanocomposite coating on the building stone.

We have demonstrated that these new coating materials are capable of the following: (1) adhering firmly to the stone surface to ensure that the conservation and self-cleaning properties of the coating have a long-term effect; (2) increasing the mechanical resistance of the stone; (3) providing proven self-cleaning properties to the stone coating; and (4) providing hydrophobic properties to the coating. We have also shown that commercial titania particles applied as a water dispersion on stone do not create an effective coating that adheres to the substratum; therefore, such dispersions are of no practical use for protecting stonework.

Lastly, we have characterized the pore structure of the new material, and have proposed a model describing how titania particles are dispersed in a silica matrix composed of silica particles. We have also demonstrated that the mesoporous structure thus created enhances the self-cleaning properties of the material, compared with the effect produced by a material comprising similar particles embedded in a microporous silica matrix.

ASSOCIATED CONTENT

Supporting Information. Nitrogen adsorption isotherms and BJH pore size distribution for P25 particles under study; FTIR spectra for TES40 after an elapsed time of 8 months; Photographs of total color variation of the surfaces of stone samples treated with the coatings under study. The samples were previously stained with methylene blue and then irradiated with UV light (λ = 365 nm) for more than 800 h. This material is available free of charge via the Internet at http://pubs.acs.org.

AUTHOR INFORMATION

Corresponding Author

*Phone: (34)956016331; Fax: (34)956016471; E-mail: mariajesus.mosquera@uca.es.

ACKNOWLEDGMENT

We are grateful for financial support from the Spanish government/FEDER-EU (Project MAT2010-16206), and the government of Andalusia (project TEP-6386 and Group TEP-243). We also thank the company Tino Stone S.A. for financial support under a research contract. L.P. thanks the Fundação Ciência e Tecnologia for his predoctoral grant (SFRH/BD/43492/2008). We also thank Lidia Esther Chinchilla for assistance with the HAADF-STEM micrographs. Finally, we express our gratitude to Evonik for supplying P25 particles.

REFERENCES

(1) Fujishima, A.; Rao, T.; Tryk, D. *J. Photochem. Photobiol. C* **2000**, *1*, 1–21.
(2) Hashimoto, K.; Irie, H.; Fujishima, A. *AAPPS Bull.* **2007**, *17*, 12–28.
(3) Fujishima, A.; Honda, K. *Nature* **1972**, *238*, 37–38.
(4) Mills, A.; Hill, G.; Bhopal, S.; Parkin, I. P.; ÓNeill, S. A. *J. Photochem. Photobiol. A* **2003**, *160*, 185–194.
(5) Vicente, J. P.; Gacoin, T; Barboux, P.; Boilot, J. P.; Rondet, M.; Gueneau, L. *Int. J. Photoenergy* **2003**, *5*, 95–98.
(6) Puzenat, E.; Pichat, P. *J. Photochem. Photobiol. A* **2003**, *160*, 127–133.
(7) Aprile, C.; Corma, A.; García, H. *Phys. Chem. Chem. Phys.* **2008**, *10*, 769–783.
(8) Álvaro, M.; Aprile, C.; Benítez, M.; Carbonell, E.; García, H. *J. Phys. Chem. B* **2006**, *110*, 6661–6665.
(9) Chen, J.; Poon, C. S. *Build. Environ.* **2009**, *44*, 1899–1906.
(10) Poulios, I.; Spathis, P.; Grigoriadou, A.; Delidou, K.; Tsoumparis, P. *J. Environ. Sci. Health A* **1999**, *34*, 1455–1471.
(11) Rao, K.; Subrahmanyam, M.; Boule, P. *Appl. Catal. B: Environ.* **2004**, *49*, 239–249.
(12) Mosquera, M. J.; de los Santos, D. M.; Montes, A.; Valdez-Castro, L. *Langmuir* **2008**, *24*, 2772–2778.
(13) Mosquera, M. J.; De los Santos, D.; Rivas, T. *Langmuir* **2010**, *26*, 6737–6745.
(14) Illescas, J. F.; Mosquera, M. J. *J. Phys. Chem. C* **2011**, *115*, 14624−14634.
(15) Suzuki, N.; Jiang, X.; Radhakrishnan, L.; Takai, K.; Shimasaki, K.; Huang, Y. T.; Miyamoto, N.; Yamauchi, Y. *Bull. Chem. Soc. Jpn.* **2011**, *84*, 812–817.
(16) Yamauchi, Y.; Takeuchi, F.; Todoroki, S.; Sakka, Y.; Inoue, S. *Chem. Lett.* **2008**, *37*, 72–73.
(17) Crepaldi, E. L.; de Soler-Illia, G. J.; Grosso, D.; Cagnol, F.; Ribot, F.; Sanchez, C. *J. Am. Chem. Soc.* **2003**, *125*, 9770–9786.
(18) Reddy, E. P.; Sun, B.; Smirniotis, P. G. *J. Phys. Chem. B* **2004**, *108*, 17198–17205.
(19) López-Muñoz, M. J.; van Grieken, R.; Aguado, J.; Marugán, J. *Catal. Today* **2005**, *101*, 307–314.
(20) Allain, E; Besson, S.; Durand, C.; Moreau, M.; Gacoin, T.; Boilot, J. P. *Adv. Funct. Mater.* **2007**, *17*, 549–554.
(21) Inumaru, K.; Yasui, M.; Kasahara, T.; Yamaguchi, K.; Yasuda, A.; Yamanaka, S. *J. Mater. Chem.* **2011**, *21*, 12117−12125.
(22) Uchiyama, H.; Suzuki, K.; Oaki, Y.; Imai, H. *Mater. Sci. Eng., B* **2005**, *123*, 248–251.
(23) Shibata, H.; Ohkubo, T.; Kohno, H.; Rangsunvigit, P.; Sakai, H.; Abe, M. *J. Photochem. Photobiol. A* **2006**, *181*, 357–362.
(24) Inumaru, K.; Kasahara, T.; Yasui, M.; Yamanaka, S. *Chem. Commun.* **2005**, 2131–2133.
(25) Ling, L.; Phang, I.; Vancso, G.; Huskens, J.; Reinhoudt, D. *Langmuir* **2009**, *25*, 3260–3263.
(26) ISO 2409; Paints and varnishes. Cross-cut test. ISO, 2007.
(27) UNE-EN 1925; Natural Stone test methods. Determination of water absorption coefficient by capillarity. *AENOR*, 1999.
(28) Berns, R. S. *Billmeyer and Saltzman's Principles of Color Technology*; Wiley-Interscience: New York, 2000.
(29) Tatsuma, T.; Tachibana, S.; Tetsuya, M.; Tryk, D.; Fujishima, A. *J. Phys. Chem. B* **1999**, *103*, 8033–8035.
(30) ISO 10678; Fine ceramics (advanced ceramics, advanced technical ceramics); Determination of photocatalytic acitivity of surfaces in an aqueous medium by degradation of methylene blue. *ISO*, 2010.
(31) Mikulasek, P.; Wakeman, R. J.; Marchant, J. Q. *Chem. Eng. J.* **1997**, *67*, 97–102.
(32) Widegren, J.; Bergström, L. *J. Am. Ceram. Soc.* **2002**, *85*, 523–528.
(33) Kosmulski, M.; Prochniak, P.; Rosenholm, J. B. *J. Phys. Chem. C* **2009**, *113*, 12806–12810.
(34) Mosquera, M. J.; de los Santos, D. M.; Valdez-Castro, L.; Esquivias, L. *J. Non-Cryst. Solids* **2008**, *354*, 645–650.
(35) Li, Y.; Kim., S. J. *J. Phys. Chem. B* **2005**, *109*, 12309–12315.
(36) Kruk, M.; Jaroniec, M. *Chem. Mater.* **2001**, *13*, 3169–3183.
(37) Barret, E. P.; Joyner, L. G.; Halenda, P. P. *J. Am. Chem. Soc.* **1951**, *73*, 373–380.
(38) Tellez, L.; Rubio, J.; Rubio, F.; Morales, E.; Oteo, J. L. *J. Mater. Sci.* **2003**, *38*, 1773–1780.
(39) Fidalgo, A.; Ilharco, L. M. *J. Non-Cryst. Solids* **2004**, *348*, 128–137.
(40) Whang, C. M.; Yeo, S. C.; Kim, Y. H. *Bull. Korean Chem. Soc.* **2001**, *22*, 1366–1370.
(41) Ferreira, A. P.; Delgado, J. *J. Cultural Heritage* **2008**, *9*, 38–53.
(42) Horiuchi, Y.; Ura, H.; Kamegawa, T.; Mori, K.; Yamashita, H. *J. Phys. Chem. C* **2011**, *115*, 15410–15415.
(43) Mills, A.; Wang, J. *J. Photochem. Photobiol. A* **1999**, *127*, 123–134.
(44) Mrowetz, M.; Balcerski, W.; Colussi, A. J.; Hoffmann, M. R. *J. Phys. Chem B* **2004**, *108*, 17269–17273.
(45) Mosquera, M. J.; Pinho, L. Spanish Patent No. P201100741. Priority data: June 24, 2011.